Environments **2014**, *1*, 157-180; doi:10.3390/environments1020157

OPEN ACCESS

environments

ISSN 2076-3298

www.mdpi.com/journal/environments

Article

Assessing the Influence of Nonpoint Source and Discharge Changes on Water Quality in a Tidal River Estuary Using a Three-Dimensional Model

Wen-Cheng Liu [1,2,*] and Wen-Ting Chan [1]

[1] Department of Civil and Disaster Prevention Engineering, National United University, Miaoli 36003, Taiwan; E-Mail: wcliu@nuu.edu.tw

[2] National Applied Research Laboratories, Taiwan Typhoon and Flood Research Institute, Taipei 10093, Taiwan

* Author to whom correspondence should be addressed; E-Mail: wcliu@nuu.edu.tw; Tel.: +886-37-382-357; Fax: +886-37-382-367.

Received: 27 September 2014; in revised form: 18 November 2014 / Accepted: 18 November 2014 / Published: 26 November 2014

Abstract: The change of nonpoint source and freshwater discharge as a result of land use change might affect the water quality in a river. In the current study, a coupled three-dimensional hydrodynamic and water quality model was created and applied to the Danshuei River estuarine system and its adjacent coastal ocean. The hydrodynamic and water quality models were validated using observations of water surface elevation, salinity distribution and water quality state variables. The predictions of hydrodynamics, salinity, dissolved oxygen and nutrients from the model simulation quantitatively agreed with the observational data. The validated model was then used to investigate the possible effects of the nonpoint source and freshwater discharge changes at the upstream reaches on water quality conditions in the Danshuei River estuarine system. Three scenarios were investigated to predict the dissolved oxygen using model simulations. The simulated results indicated that increasing nonpoint sources at the upstream reaches degraded the dissolved oxygen under low flow conditions. However, increasing freshwater discharges at the upstream reaches would overcome the loadings of the nonpoint source, which would result in increasing the dissolved oxygen in the tidal river estuary. The model can provide a useful tool for developing management practices for nonpoint sources to protect the water quality in the estuarine system.

Keywords: land use; nonpoint source; modeling; hydrodynamics; water quality; tidal estuarine system; Danshuei River

1. Introduction

An increasing population, changes in urbanization and agricultural practices and structural landscape transformations have considerably modified the natural biogeochemical cycles of essential bio-elements on both a local and large scale [1–3]. Surface water is controlled by natural processes, such as weathering and precipitation inputs, by anthropogenic activities, such as industrial effluents and wastewater treatment facilities, and by diffuse inputs, such as runoffs from urban areas and farms. Several studies demonstrate that surface water quality has severely deteriorated in numerous countries over the past few decades because of poor land use, which is indicated by a strong relationship between the declining water quality and the increasing development of the catchment scale [4,5].

Water quality is generally linked to land use/land cover (LULC) in catchments [6], and studies have focused on their relationship with water quality variables, such as dissolved salts, suspended solids and nutrients [7–10]. These studies discovered that agricultural and urban land use strongly affect nutrients in the river water. Different methodologies have been applied to assess the effects of changes in the LULC on biogeochemical cycles, biodiversity and water quality [11–15]. For example, Wang *et al.* [16] assessed the spatial-temporal water quality to identify the LULC sources of water pollution. Kibena *et al.* [17] combined *in situ* measurements and remote sensing techniques to assess the impacts of land use activities on the water quality of the Upper Manyame River in ZimbabweBu *et al.* [18] used land use types and landscape matrices, as well as statistical and spatial analyses to determine the relationships between land use patterns and river water quality in the Taizi River Basin in China during the dry and rainy seasons of 2009. However, measuring the LULC and its rates and patterns of change correlated with the water quality are traditional measures. Erol and Randhir [19] used a watershed ecosystem model to assess the impact of land use on water quality in the Lake Egirdir watershed, Turkey. Recently, different kinds of models have been widely adopted to evaluate the influences of LULC on water quality.

Estuaries are complex ecosystems that can include wetlands and mangrove swamps along their intertidal shores. They serve as a meeting point between land and sea and occupy specific ecological niches of considerable importance. However, because of human activities, adverse effects on the estuarine ecosystem have been widely reported [20,21]. Numerical water quality models are useful in helping to understand the biological processes, nutrient loading and managing water quality conditions in aquatic systems. Deterministic models for water quality conditions are based on mass balance equations for dissolved and particulate substances in the water column, which consist of physical transport processes and biogeochemical processes. Information on the physical processes is typically obtained by applying hydrodynamic models. Once calibrated and verified against the observational data, the deterministic models then can be applied to explore a number of issues that can provide information for management practices [22,23].

Lin *et al.* [24] assessed the land use changes and their effects on land use patterns and hydrological processes at the Wu-Tu watershed in the upstream of the Keelung River Basin, but did not focus on the water quality issues. Because of urban development, the LULC in the Danshuei River watershed of northern Taiwan has been significantly changed, which resulted in an increase in the nonpoint source and discharge. A coupled three-dimensional hydrodynamic and water quality model (SELFE-WQ) was implemented to probe the influence of the increases in nonpoint source and freshwater discharge at the upstream reaches on water quality in the estuarine system. The model was validated by observations of the water surface elevation, salinity and water quality state variables. Then, the validated water quality model was used to predict the water quality for different scenarios by varying the inputs of the nonpoint source and freshwater discharge under low flow conditions.

2. Materials and Methods

2.1. Description of Study Area

The Danshuei River, along with its tributaries, is the largest river system in northern Taiwan. Its watershed encompasses 2726 km^2, and it has a combined length of 158.7 km. This river consists of three major tributaries: the Tahan Stream, the Hsintien Stream and the Keelung River (Figure 1). The mean river discharges are 38.99 m^3/s, 69.72 m^3/s and 25.02 m^3/s in the Tahan Stream, the Hsintien Stream and the Keelung River, respectively. In addition to the primary stream of the Danshuei River, the lower reaches of the three major tributaries are also affected by the tide. The principal tidal constituents of the estuary lean toward semi-diurnal tides, with a mean tidal range of 2.1 m and a spring tidal range of 3.5 m. Seawater intrusion reaches into all three tributaries, except during the period of extremely high river inflows. Generally, saltwater intrusion reaches 25–30 km from the mouth of the Danshuei River. The hydrodynamic characteristics in the system are primarily controlled by the tide, river inflow and density gradient induced by the mixing of seawater and freshwater [25,26].

The Danshuei River flows through the metropolitan area of Taipei, which has a population of approximately 6 million. A large amount of treated and untreated domestic sewage was discharged into the river system and resulted in low dissolved oxygen and high nutrient concentrations. Viable biological activities were observed only in the lowest reaches of the estuary, where the pollutant concentrations are reduced as a result of being diluted with sea water.

2.2. Hydrodynamic Model

The numerical modeling of ocean circulation at scales ranging from estuaries to ocean basins is becoming a developed field. Most modern oceanic and estuarine circulation codes solve for various forms of the three-dimensional Navier–Stokes equations and can be complemented with conservation equations for a given water volume and salt concentration. In this report, a three-dimensional, semi-implicit Eulerian–Lagrangian finite-element model (SELFE, [27]) was implemented to simulate the Danshuei River estuarine system and its adjacent coastal sea. The SELFE model solves the Reynolds stress-averaged Navier–Stokes equations, which use conservation laws for mass, momentum and salt with hydrostatic and Boussinesq approximations, to determine the free-surface elevation, three-dimensional water velocity and salinity. The SELFE model addresses the advection in transport

equations using the Eulerian–Lagrangian method. The transport equations are solved at nodes and side centers along each vertical column using a finite element method, with the mass matrix lumped to minimize numerical dispersion.

Figure 1. Danshuei River estuarine system and watershed.

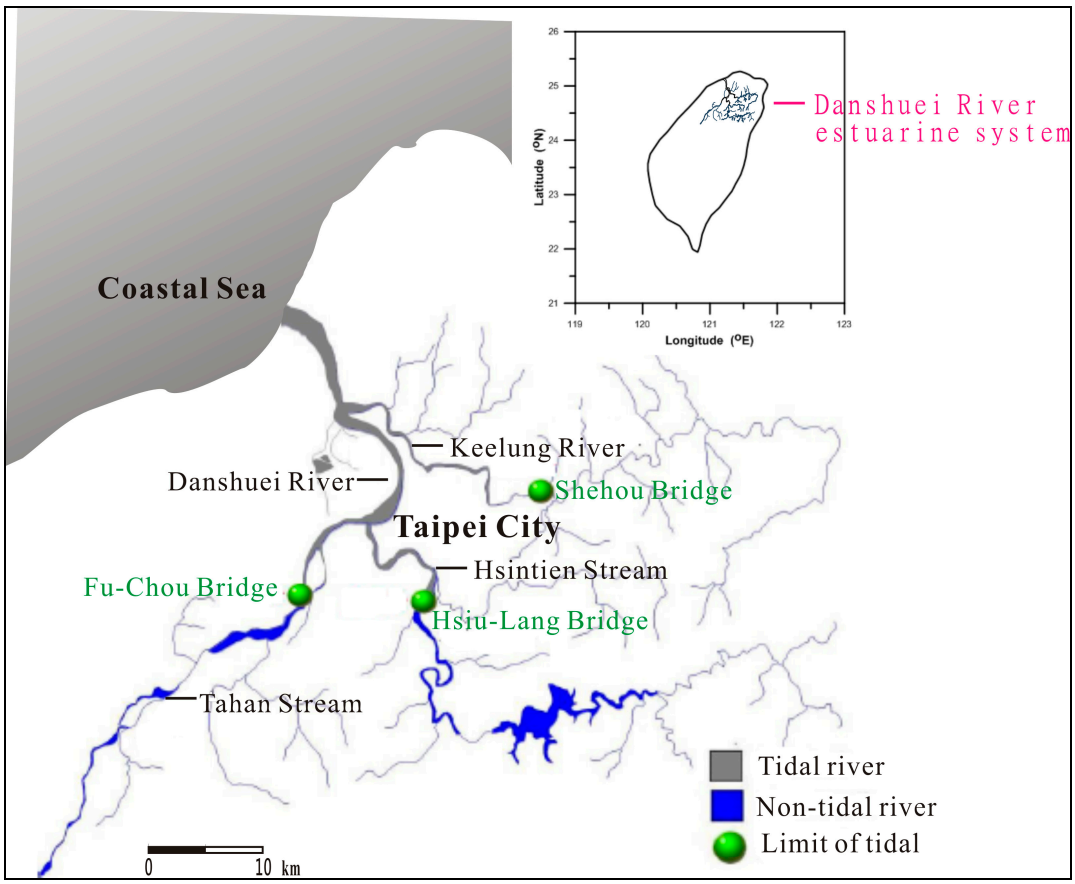

In the vertical direction, models based on terrain-following coordinates suffer from hydrostatic inconsistencies. This follows from the fact that the terrain-following coordinates do not conform to the geopotential, and the pressure gradient is evaluated as the difference between two large components that tend to cancel each other out, thus producing large discretization errors. Furthermore, these inconsistencies can be viewed as a result of efficiently evaluating the pressure at a grid point using extrapolation when steep bathymetric slopes are presented. Several remedies have been used to prevent this result, including evaluating the gradient along the Z-coordinate or applying high-order schemes [28]. In the current model, the use of a hybrid coordinate system in the vertical direction effectively prevents the hydrostatic inconsistency, because the Z-coordinates used in the deeper part of the vertical axis serve to "stabilize", while the S-coordinates are used in the upper part of the water column.

Because turbulent mixing plays a critical role in determining the stratification in the tidal estuary, several reports have documented the modeling results of turbulence mixing parameterizations. The SELFE model uses the generic length scale (GLS) turbulence closure of Umlauf and Burchard [29], which has the advantage of encompassing most of the 2.5-equation closure model ($K - \psi$). A detailed description of the turbulence closure model, the vertical boundary conditions for the momentum

equation, the numerical solution methods and the numerical stability can be found in Zhang and Baptista [27].

2.3. Water Quality Model

The water quality model used in this study was based on a three-dimensional conventional water quality analysis simulation program, called WASP5, which was originally developed by Ambrose *et al.* [30]. It is comprised of a complicated system of four interacting parts: dissolved oxygen concentration, nitrogen cycle, phosphorus cycle and phytoplankton dynamics. Eight water quality components are included: dissolved oxygen (DO), phytoplankton as carbon (PHYT), carbonaceous biochemical oxygen demand (CBOD), ammonium nitrogen (NH_4), nitrate nitrogen (NO_3), organic nitrogen (ON), ortho-phosphorus or inorganic phosphorus (OPO_4) and organic phosphorus (OP).

A mathematical formulation of the conservation of mass can be written as follows:

$$\frac{\partial C}{\partial t}+\frac{\partial (uC)}{\partial x}+\frac{\partial (vC)}{\partial y}+\frac{\partial (wC)}{\partial z}=\frac{\partial}{\partial x}(A_h\frac{\partial C}{\partial x})+\frac{\partial}{\partial y}(A_h\frac{\partial C}{\partial y})+\frac{\partial}{\partial z}(K_v\frac{\partial C}{\partial z})+S_c \quad (1)$$

where C is the concentration of the water quality components, u, v and w are the water velocity components corresponding to a Cartesian coordinate system (x, y, and z), A_h and K_v are the coefficients of the horizontal and vertical eddy diffusion, respectively, and S_c is a function that represents the internal source or sink of the water quality component.

2.4. Model Implementation

In the current study, the bathymetry and topography data of the Taiwan Strait and the Danshuei River estuarine system were obtained from the Ocean Data Bank and Water Resources Agency in Taiwan. The deepest point within the study area is 110 m (below mean sea level) near the northeast corner of the computational domain (Figure 2). The model mesh for the Danshuei River estuarine system and its adjacent coastal sea consists of 5119 elements (Figure 2). To meet the accuracy requirements, a fine-grid resolution was used locally, while a coarse resolution was implemented away from the region of interest. In this computational domain, the mesh size varied from 6000 m in the Taiwan Strait to 40 m in the upper reach of the Danshuei River estuarine system. In the vertical direction, ten Z-levels and ten evenly spaced S-levels were specified at each horizontal grid, *i.e.*, the thickness of the cell depended on the bottom elevation of each grid. A 120-second time step was used in our simulations without any signs of numerical instability.

3. Model Validation

3.1. Tidal Elevation

The calibrated and verified model procedures were performed for daily freshwater discharges at the upstream boundaries in the Tahan Stream, Hsintien Stream and Keelung River in 2010. The model was run for a one-year simulation. Before the one-year simulated run, the model was spun up fifteen days to reach an equilibrium state. These conditions served to investigate the model response to the interactions of tidal forcing and varying river discharge. First, the coupled hydrodynamic and water

quality model was calibrated with hydrodynamics (*i.e.*, water surface and salinity) and then was calibrated and verified with water quality variables. The manual calibration procedure was conducted in the model simulation. The comparison between the model simulation and the measured water surface elevations is presented in Figure 3 at the following tidal gauge stations: Danshuei River mouth, Tu-Ti-Kung-Pi, Taipei Bridge, Hsin-Hai Bridge, Chung-Cheng Bridge, Ba-Ling Bridge and Ta-Chih Bridge (the locations are provided in Figure 2) for the period of 27 February to 8 March 2010. Generally, the modeling results accurately reproduced the water level variations. The mean absolute errors and the root mean square errors of the difference between the measured hourly surface elevations and the computed surface elevations during the period of 27 February to 8 March 2010, are provided in Table 1. Through the model validation with tidal elevation, a constant bottom roughness height (z_o = 0.005 m) is used in the model simulation.

Figure 2. Topography of the Danshuei River estuarine system and its adjacent coastal and unstructured grid for the computational domain.

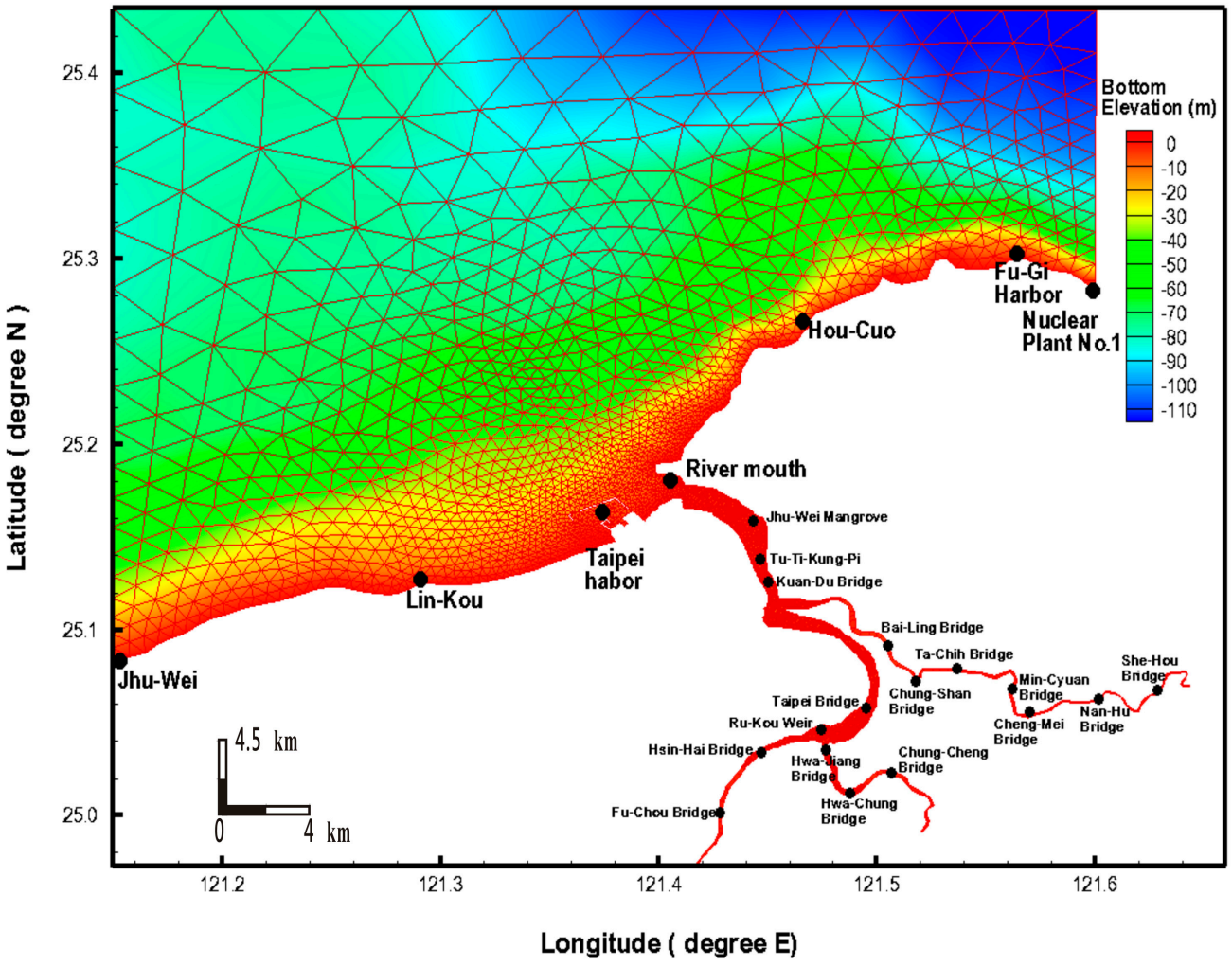

Figure 3. Comparison between measured and simulated water surface elevation during the period of 27 February to 8 March 2010, at the (**a**) Danshuei River mouth, (**b**) Tu-Ti-Kung-Pi, (**c**) Taipei Bridge, (**d**) Hsin-Hai Bridge, (**e**) Chung-Cheng Bridge, (**f**) Bai-Ling Bridge and (**g**) Ta-Chih Bridge.

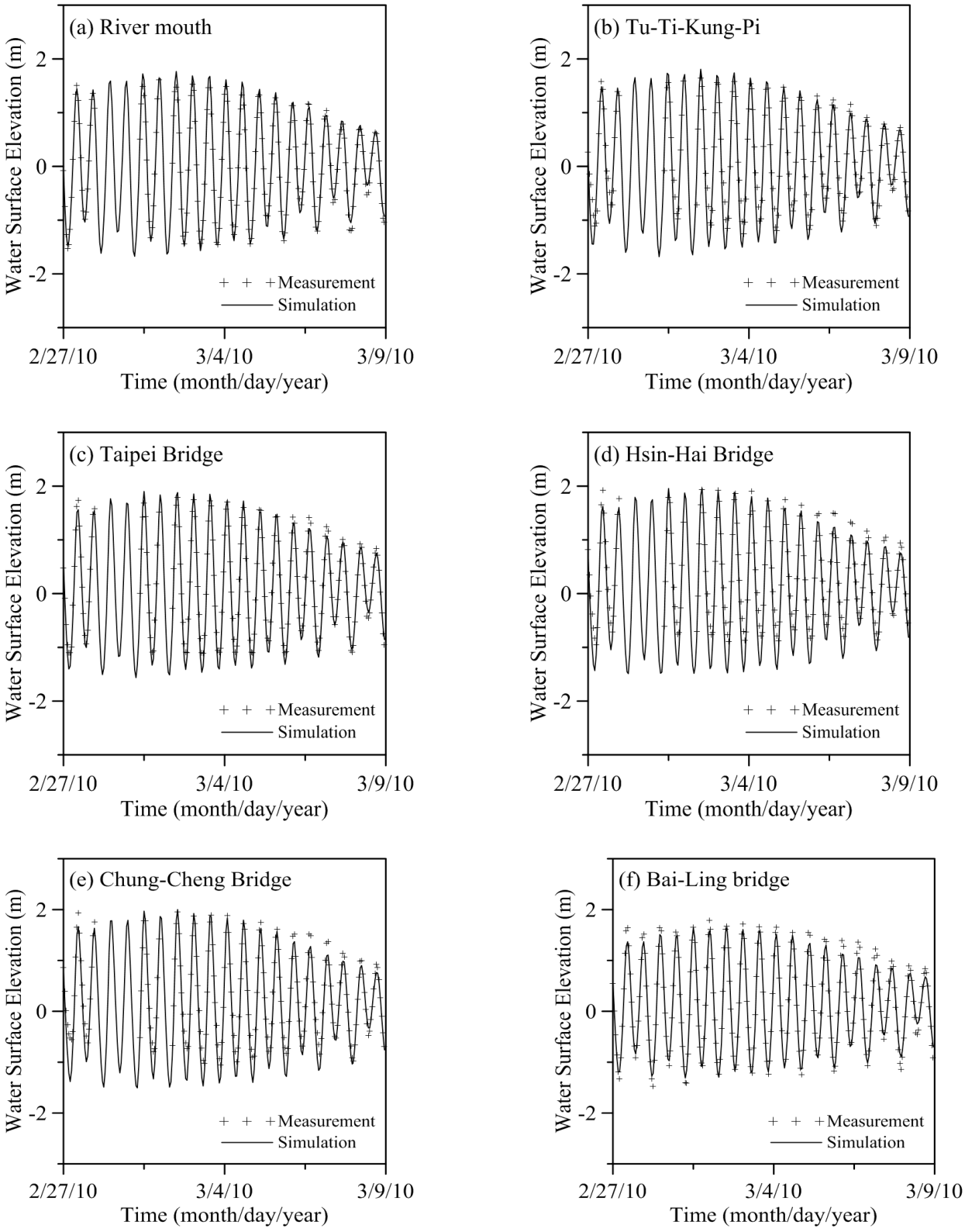

Figure 3. *Cont.*

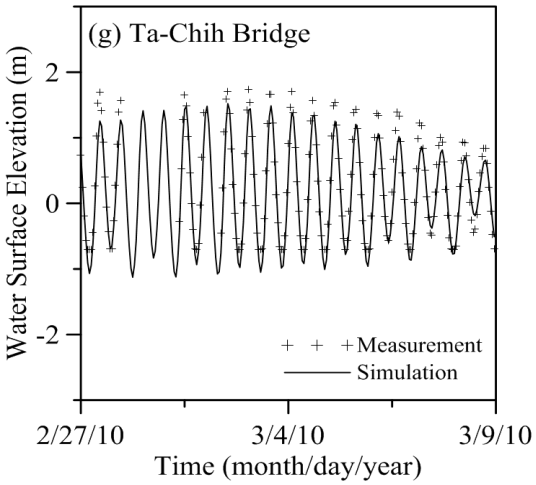

Table 1. Statistical error between simulated and measured water surface elevations at seven tidal stations during the period of 27 February to 8 March 2010.

Gauge Station	Statistical Error	Value
Danshuei River mouth	AME (m)	0.10
	RMSE (m)	0.12
Tu-Ti-Kung-Pi	AME (m)	0.24
	RMSE (m)	0.32
Taipei Bridge	AME (m)	0.14
	RMSE (m)	0.17
Hsin-Hai Bridge	AME (m)	0.24
	RMSE (m)	0.32
Chung-Cheng Bridge	AME (m)	0.20
	RMSE (m)	0.26
Ba-Ling Bridge	AME (m)	0.12
	RMSE (m)	0.15
Ta-Chih Bridge	AME (m)	0.19
	RMSE (m)	0.25

Notes: AME, absolute mean error; RMSE, root mean square error.

3.2. Salinity Distribution

The salinity distributions reflect the combined results of all processes, including density circulation and mixing processes, which, in turn, control the density circulation and modify the mixing processes. In the current study, the salinity distribution along the Danshuei River-Tahan Stream, which was collected by the Water Resources Agency in Taiwan, was used for model validation. The salinities of the open boundaries in the coastal sea were set to 35 *ppt*. Furthermore, the upstream boundary conditions at the three tributaries (Tahan Stream, Hsintien Stream and Keelung River) were specified with daily freshwater discharges; thus, the salinity at the upstream boundaries was set to 0 *ppt*. The simulated salinity distribution compared favorably with the salinity measurements along the Danshuei River-Tahan Stream during the flood and ebb tides on 26 November 2010, as indicated in Figure 4. It should be noted that the salinity field data were measured at 0.5 m below the water surface, and the

simulated salinity was instead presented as the top layer and the bottom layer. Because ten Z-levels and ten evenly spaced S-levels were specified in the vertical direction for model simulation, the water depths at the top and bottom layer were different along the Danshuei River mouth. The absolute mean error and the root mean square error are 2.71 *ppt* and 3.72 *ppt* during the flood tide, respectively, and 0.49 *ppt* and 0.67 *ppt* during the ebb tide, respectively. The simulated results indicate that the model performs better for the ebb tide compared to that of the flood tide.

Figure 4. Comparison between measured and simulated salinities along the Danshuei River-Tahan Stream on 26 November 2010, during the (**a**) flood tide and (**b**) ebb tide.

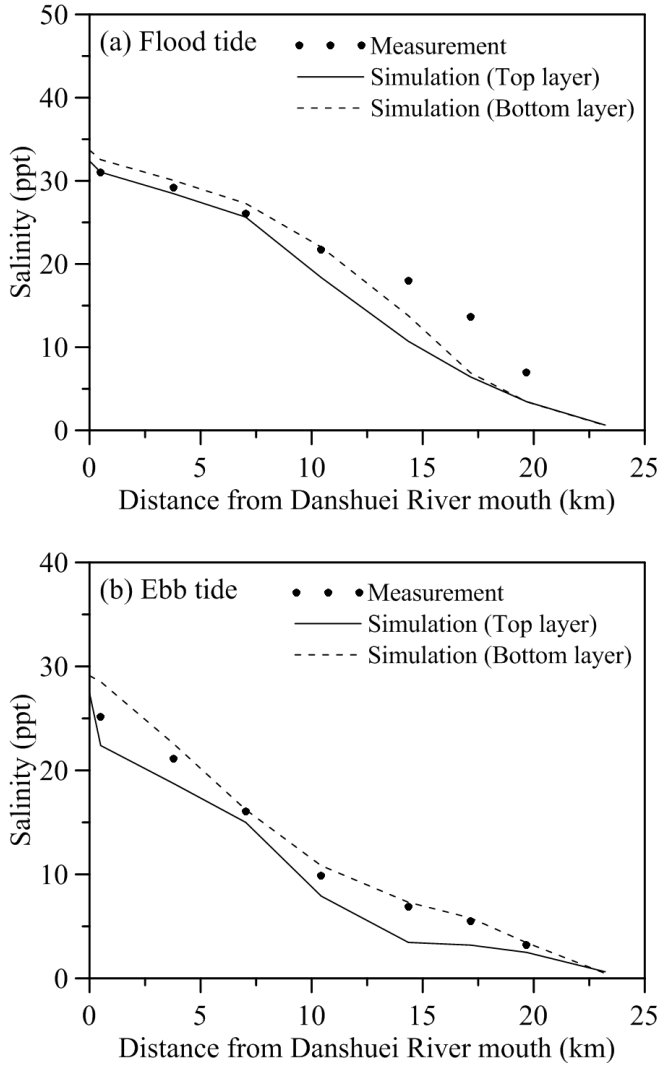

3.3. Water Quality State Variables

Adjacent to the metropolitan city of Taipei, it is believed that the spatial trend of the deteriorated water quality is primarily attributed to the wastewaters directly discharged into the river channels [31]. Successive efforts were made to estimate the point source loadings that Montgomery Watson Harza (MWH) [32] used in the following water quality simulations. The daily freshwater discharges from 2010 were applied at the upstream boundaries at the Tahan Stream, Hsintien Stream and Keelung River. The five-constituent tide used to generate the time series tidal level was used at the ocean

boundaries. The concentrations of the water quality state variables, including ammonium nitrogen, total nitrogen, total phosphorus, carbonaceous biochemical oxygen demand, dissolved oxygen and chlorophyll *a*, at the river and ocean boundaries were established based on the monthly measurement performed by the Taiwan Environmental Protection Administration (TEPA).

Two measured datasets were collected on 1 March and 1 June 2010, used for model calibration, while the other two datasets were collected on 3 September and 2 December 2010, adopted for model verification. The model parameters were initially estimated from the literature [33]. These parameters were adjusted and tuned until a reasonable reproduction of the field data was obtained at the observation stations. Table 2 indicates the coefficients adopted for water quality simulations. Because of the constraint of space, thee longitudinal water quality distributions predicted by the water quality model on 1 March 2010, for the Danshuei River-Tahan Stream, Hsintien Stream and Keelung River are provided only in Figure 5 to Figure 7, respectively. The observational stations shown in Figures 5–7 refer to Figure 2. The water quality distributions of the dissolved oxygen, carbonaceous biochemical oxygen demand, ammonium nitrogen, total phosphorus and nitrate nitrogen concentrations at the top and bottom layers along the river channels are presented in the figures along with the observations at the monitoring stations. Because there were no measured nitrate nitrogen data, the simulated results at the top and bottom layers are only presented in Figure 5e. Figure 5a indicates that both the concentrations predicted by the model and the observed dissolved oxygen concentrations along the Danshuei River-Tahan Stream depict a decreasing trend from the Danshuei River mouth to the Hsin-Hai Bridge. In the lower estuary, the dissolved oxygen concentrations increase toward the river mouth as a result of seawater dilution. The lowest dissolved oxygen concentration occurs at the Hsin-Hai Bridge. The carbonaceous biochemical oxygen demand, ammonium nitrogen and total phosphorous all indicate the same spatial trends along the river channel from the Danshuei River to the Tahan Stream (Figures 5b–d). The concentrations increase from the mouth of the Danshuei River, reach a maximum at the Hsin-Hai Bridge and then gradually decrease towards the Fu-Chou Bridge. The maximum concentrations of these three water quality state variables all occur at the Hsin-Hai Bridge, which results in the lowest dissolved oxygen. Figures 5a–d indicates that the model generally captured the spatial trends of the observed longitudinal distributions, but could not mimic the observed dissolved oxygen concentration at the lower reaches.

Figure 6 illustrates the longitudinal water quality distributions along the Hsintien Stream. Both the observed data and the model predictions indicate that the water quality conditions degrade as one approaches the river mouth, where it joins the main stem of the Danshuei River, the dissolved oxygen decreases and the organic carbon, ammonium nitrogen and total phosphorus increase (Figures 6a–d). The model accurately captures the observed carbonaceous biochemical oxygen demand, ammonium nitrogen and total phosphorous along the Hsintien Stream.

Table 2. Coefficients adopted in the water quality model.

Coefficients	Value	Unit
Deoxygenation rate at 20 °C	0.16	day^{-1}
Nitrification rate at 20 °C	0.13	day^{-1}
Phytoplankton respiration rate at 20 °C	0.6	day^{-1}
Denitrification rate at 20 °C	0.09	day^{-1}
Organic nitrogen mineralization at 20 °C	0.075	day^{-1}
Organic phosphorus mineralization at 20 °C	0.22	day^{-1}
Optimum phytoplankton growth rate at 20 °C	2.5	day^{-1}
The morality rate of phytoplankton at 20 °C	0.003	day^{-1}
Half-saturation constant for oxygen limitation of carbonaceous deoxygenation	0.5	mg O_2 L^{-1}
Half-saturation constant for oxygen limitation of nitrification	0.5	mg O_2 L^{-1}
Half-saturation constant for uptake of inorganic nitrogen	25	μg N L^{-1}
Half-saturation constant for uptake of inorganic phosphorus	1	μg P L^{-1}
Half-saturation constant for oxygen limitation of denitrification	0.1	mg O_2 L^{-1}
Half-saturation constant of phytoplankton limitation of phosphorus recycling	1	mg C L^{-1}
Sediment oxygen demand at 20 °C	3.5	g/m^2−day
Optimal solar radiation rate	250	langleys/day
Total daily solar radiation	300	langleys/day
Ratio of nitrogen to carbon in phytoplankton	0.25	mg N/mg C
Ratio of phosphorus to carbon in plankton	0.025	mg P/mg C
Organic carbon (as CBOD) decomposition rate at 20 °C	0.21	day^{-1}
Anaerobic algae decomposition rate at 20 °C	0.01	day^{-1}
Denitrification rate at 20 °C	0.01	day^{-1}
Organic nitrogen decomposition rate at 20 °C	0.01	day^{-1}
Organic phosphorus decomposition rate at 20 °C	0.01	day^{-1}
Benthic NH4 flux	0.04	mg N day^{-1}
Benthic NO3 flux	0.003	mg N day^{-1}
Benthic PO4 flux	0.005	mg P day^{-1}
Ratio of nitrogen to carbon	0.01	mg N/mg C
Ratio of phosphorus to carbon	0.01	mg P/mg C

Figure 5. Comparison between measured and simulated water quality distribution along the Danshuei River to Tahan Stream on 1 March 2010: (**a**) dissolved oxygen (DO); (**b**) carbonaceous biochemical oxygen demand (CBOD); (**c**) NH_4; (**d**) total phosphorus (TP); and (**e**) NO_3 (simulated result shown only as no NO_3 measurement).

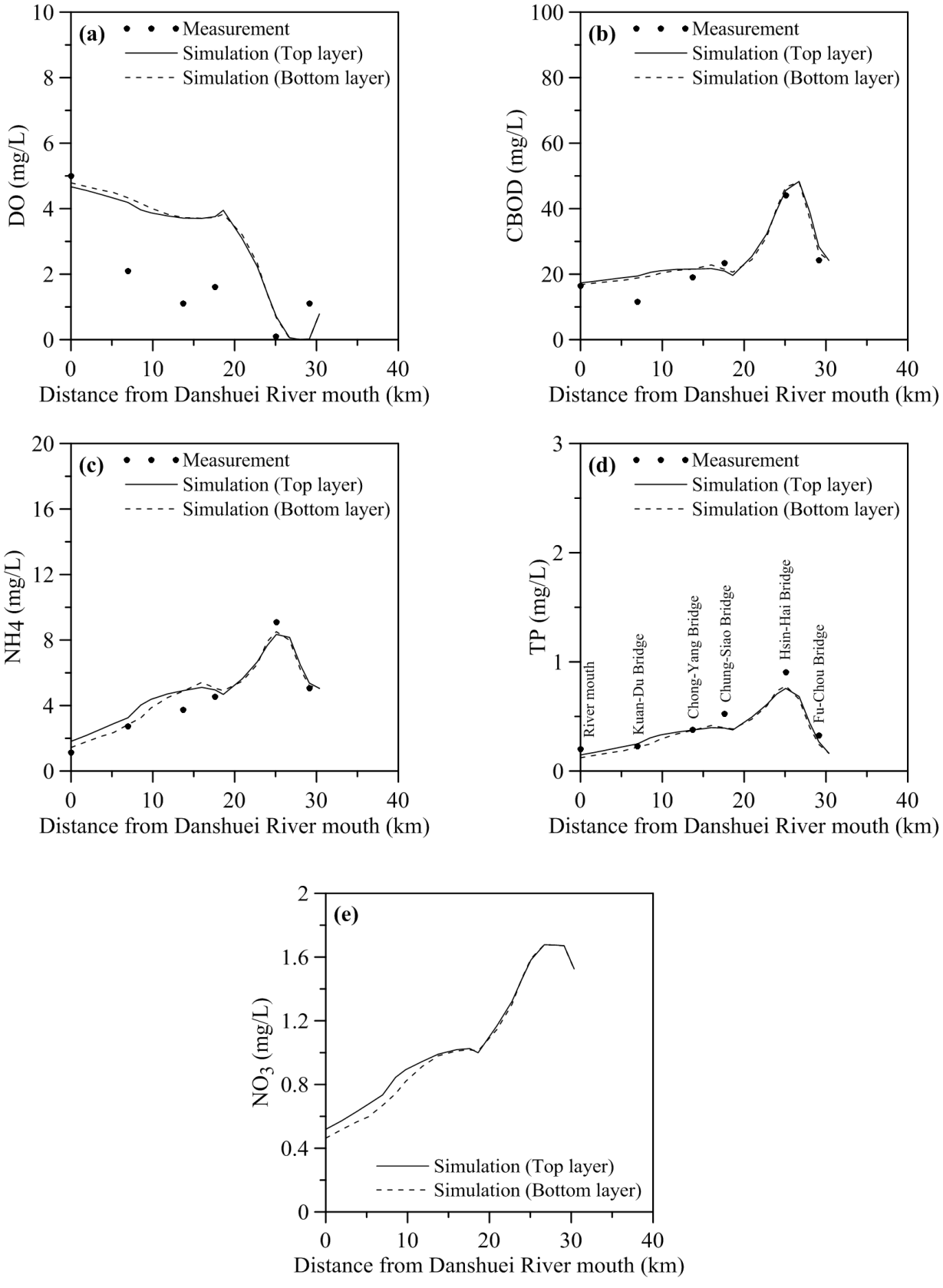

Figure 6. Comparison between measured and simulated water quality distribution along the Hsintien Stream on 1 March 2010: (**a**) DO; (**b**) CBOD; (**c**) NH_4; (**d**) TP; and (**e**) NO_3 (simulated result shown only as no NO_3 measurement).

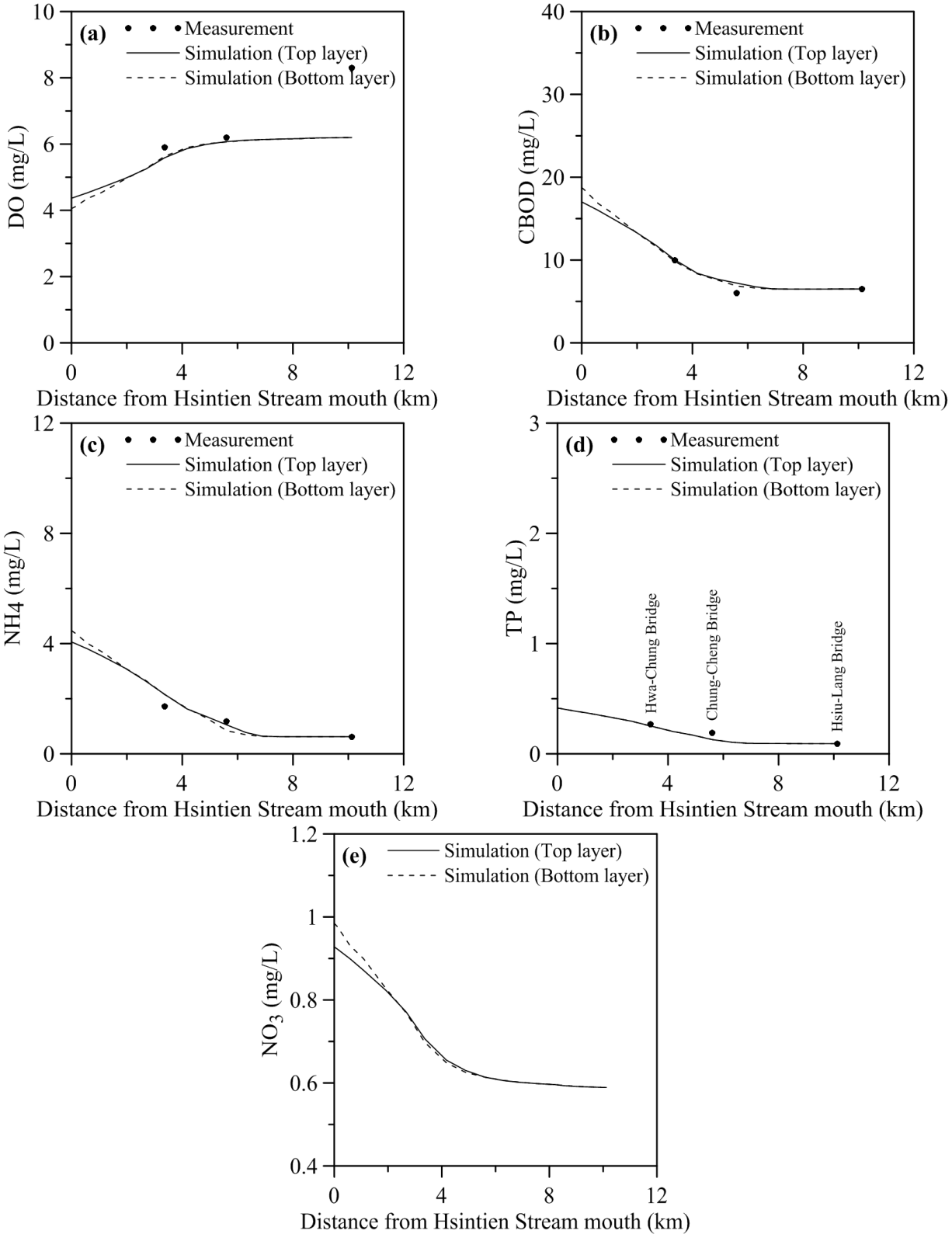

Figure 7. Comparison between measured and simulated water quality distribution along the Keelung River on 1 March 2010: (**a**) DO; (**b**) CBOD; (**c**) NH_4; (**d**) TP; and (**e**) NO_3 (simulated result shown only as no NO_3 measurement).

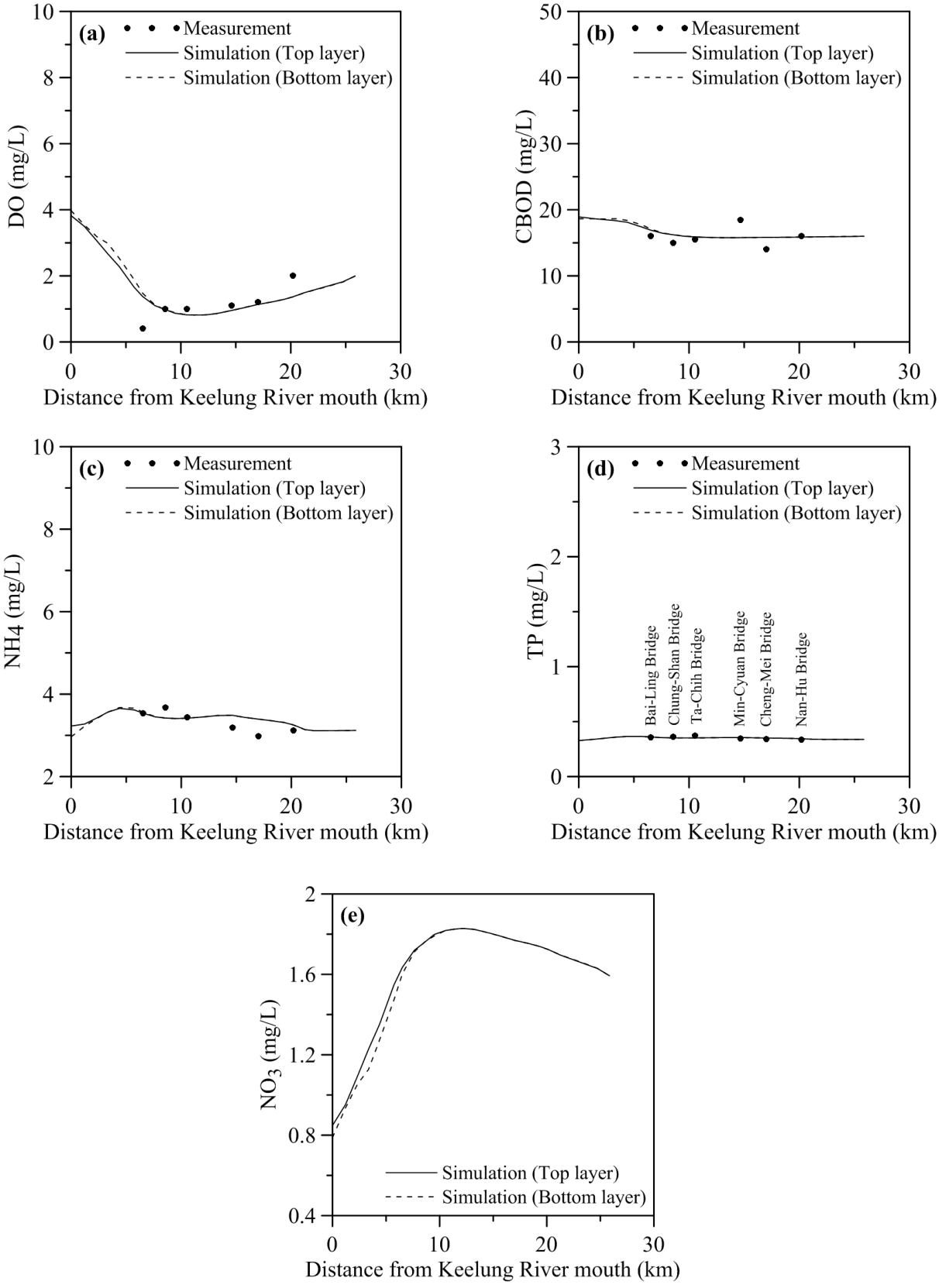

The longitudinal water quality distribution along the Keelung River (Figure 7) indicates that there were significant nutrient loadings discharged into the river section near the Bai-Ling Bridge, which is where the lowest dissolved oxygen in the Keelung River was observed. The model cannot actually mimic this lowest observed dissolved oxygen concentration, but does accurately match the observed carbonaceous biochemical oxygen demand, ammonium nitrogen and total phosphorous quite well along the Keelung River (Figures 7a–d). The comparison of simulated and measured nitrate nitrogen concentration is not possible, because there were no measured nitrate nitrogen data. The model performance with statistical errors, including the absolute mean error and the root mean square error, on 1 March, 1 June, 3 September and 2 December 2010, are illustrated in Tables 3–6, respectively.

Table 3. Statistical error between simulated and measured water quality variables on 1 March 2010.

Water Quality Variable	Danshuei River-Tahan Stream		Hsintien Stream		Keelung River	
	AME (mg/L)	RMSE (mg/L)	AME (mg/L)	RMSE (mg/L)	AME (mg/L)	RMSE (mg/L)
Dissolved oxygen	1.48	1.72	0.84	1.23	0.35	0.50
Carbonaceous biochemical oxygen demand	3.06	3.76	0.37	0.60	1.14	1.45
Ammonium nitrogen	0.56	0.64	0.23	0.29	0.19	0.24
Total phosphorus	0.06	0.07	0.02	0.04	0.01	0.01

Notes: AME, absolute mean error; RMSE, root mean square error.

Table 4. Statistical error between simulated and measured water quality variables on 1 June 2010.

Water Quality Variable	Danshuei River-Tahan Stream		Hsintien Stream		Keelung River	
	AME (mg/L)	RMSE (mg/L)	AME (mg/L)	RMSE (mg/L)	AME (mg/L)	RMSE (mg/L)
Dissolved oxygen	0.42	0.49	1.58	2.06	0.76	0.80
Carbonaceous biochemical oxygen demand	0.73	0.99	0.62	0.99	1.20	1.61
Ammonium nitrogen	0.14	0.24	0.33	0.50	0.22	0.25
Total phosphorus	0.03	0.05	0.04	0.05	0.03	0.04

Notes: AME, absolute mean error; RMSE, root mean square error.

Table 5. Statistical error between simulated and measured water quality variables on 3 September 2010.

Water Quality Variable	Danshuei River-Tahan Stream		Hsintien Stream		Keelung River	
	AME (mg/L)	RMSE (mg/L)	AME (mg/L)	RMSE (mg/L)	AME (mg/L)	RMSE (mg/L)
Dissolved oxygen	0.62	0.77	2.06	2.56	0.51	0.59
Carbonaceous biochemical oxygen demand	1.49	2.46	0.23	0.36	2.68	3.31
Ammonium nitrogen	0.29	0.35	0.32	0.54	0.16	0.19
Total phosphorus	0.05	0.08	0.06	0.10	0.07	0.08

Notes: AME, absolute mean error; RMSE, root mean square error.

Table 6. Statistical error between simulated and measured water quality variables on 2 December 2010.

Water Quality Variable	Danshuei River-Tahan Stream		Hsintien Stream		Keelung River	
	AME (mg/L)	RMSE (mg/L)	AME (mg/L)	RMSE (mg/L)	AME (mg/L)	RMSE (mg/L)
Dissolved oxygen	0.63	0.88	2.17	3.47	0.91	0.98
Carbonaceous biochemical oxygen demand	2.21	2.79	1.79	2.29	2.02	2.51
Ammonium nitrogen	0.36	0.54	0.52	0.74	0.15	0.19
Total phosphorus	0.07	0.10	0.08	0.12	0.008	0.01

Notes: AME, absolute mean error; RMSE, root mean square error.

4. Model Application: System Response to Nonpoint Source and Discharge Changes

The Danshuei River watershed can be classified into nine land uses, which include forest, agriculture, stream and reservoir, residential, transportation, grass land, bare soil, bush, and others. The percentages of 89% and 4.5% are occupied by forest and agriculture, respectively. To examine the system's response to a change of nonpoint source loadings and discharges from the upstream watershed, the validated model was used to predict the dissolved oxygen distribution under low flow conditions. To perform the model prediction, the five-constituent tide at the ocean boundaries was used to force the model simulation. The concentrations of the water quality state variables, *i.e.*, ammonium nitrogen, total nitrogen, total phosphorus, carbonaceous biochemical oxygen demand, dissolved oxygen and chlorophyll *a*, at the river and ocean boundaries were established based on the mean values calculated from the measured water quality data, which were observed and collected from 2003 to 2013 by the TEPA (Table 7). Because the low flow could have significant influence on the water quality condition in the river, it was specified for model simulation. A Q_{75} (a flow that equals or exceeded 75% of the time) flow condition is widely used in Taiwan to represent the designed low flow for water quality model simulation. The river discharges at the tidal limits of the three major tributaries, *i.e.*, Tahan Stream, Hsintien Stream and Keelung River, were determined using a Q_{75} low flow condition. The Q_{75} river flows at the upstream reaches of the Tahan Stream, Hsintien Stream and Keelung River are 3.36, 14.23 and 3.33 m^3/s, respectively. In order to comprehend the impact of the change in nonpoint sources loadings due to a change in land use, the point source loadings were kept the same with model calibration and verification (Section 3.3). Table 8 presents the estimated nonpoint source loadings for different water qualities under the Q_{75} flow condition.

Three scenarios, as presented in Table 9, were adopted to respond to the change of nonpoint sources and freshwater discharges and to predict the dissolved oxygen distribution in the tidal estuarine system. To operate the model prediction for the different scenarios, we used 10%–100% nonpoint source increases and 10%–100% Q_{75} flow increases to represent the increasing ratio of water quality concentrations at the upstream boundaries and the river flows at the upstream boundaries, respectively, as a result of the change in land use. The incremental ratio for the nonpoint source and Q_{75} flow was set to 10% for each model run.

Table 7. The water quality specified at the upstream and ocean boundaries for model simulation.

Water Quality State Variable	Tahan Stream	Hsintien Stream	Keelung River	Open Boundary (Ocean)
Ammonia nitrogen (mg/L)	20.2	8.6	15.9	5.0
Total nitrogen (mg/L)	21.5	0.37	17.4	5.1
Total phosphorus (mg/L)	0.8	0.20	0.30	0.08
Carbonaceous biochemical oxygen demand (mg/L)	2.3	0.81	2.5	0.07
Dissolved Oxygen (mg/L)	5.5	7.7	6.9	6.7
Chlorophyll *a* (μg/L)	1	1	1	1

Table 8. Estimated nonpoint source loadings under Q_{75} flow condition.

Water Quality State Variable	Tahan Stream (Kg/day)	Hsintien Stream (Kg/day)	Keelung River (Kg/day)
Ammonia nitrogen	5863.3	10,518.1	4586.1
Total nitrogen	6251.9	11,517.7	4999.3
Total phosphorus	233.52	250.8	85.2
Carbonaceous biochemical oxygen demand	663.3	998.3	717.3
Dissolved Oxygen	1595.7	9523.5	1999.6
Chlorophyll *a*	0.29	1.23	0.28

Table 9. Description of different scenarios for model prediction.

Scenario	Simulation Condition
Scenario 1	10%~100% increasing ratio of nonpoint source and Q_{75} flow at upstream boundaries (the increment ratio is 10%)
Scenario 2	50% increasing ratio of nonpoint source and 10%~100% increasing ratio of the Q_{75} flow at upstream boundaries (the increment ratio is 10%)
Scenario 3	100% increasing ratio of nonpoint source and 10%~100% increasing ratio of the Q_{75} flow at upstream boundaries (the increment ratio is 10%)

Figure 8 presents the prediction of the dissolved oxygen distribution along the Danshuei River to the Tahan Stream, the Hsintien Stream and the Keelung River for the baseline case and different cases. In the figure, Line 1, Line 2 and Line 3 represent a 50% increasing ratio for the nonpoint source, a 50% increasing ratio for the nonpoint source, a 50% increasing ratio for the Q_{75} flow, a 100% increasing ratio for nonpoint source and a 50% increasing ratio for the Q_{75} flow, respectively. It can be determined that the dissolved oxygen in Line 2 is higher compared to that of the baseline in the Danshuei River to Tahan Stream, while the dissolved oxygen distribution in both Lines 2 and 3 is higher compared to that of the baseline. The dissolved oxygen distribution in all of the lines is lower than the baseline. This result indicates that the nonpoint source and the freshwater discharge in the upstream reaches would dominate the dissolved oxygen distribution in the primary stream and the two tributaries. Increasing the nonpoint source worsens the water quality, while increasing the freshwater discharge enhances the dissolved oxygen.

Figure 8. Predicting dissolved oxygen distribution for baseline and different cases along the (**a**) Danshuei River to Tahan Stream, (**b**) Hsintien Stream and (**c**) Keelung River. (Note that Line 1 represents a 50% increasing ratio for the nonpoint source, Line 2 represents a 50% increasing ratio for the nonpoint source and a 50% increasing ratio for the Q_{75} flow and Line 3 represents a 100% increasing ratio for the nonpoint source and a 50% increasing ratio for the Q_{75} flow).

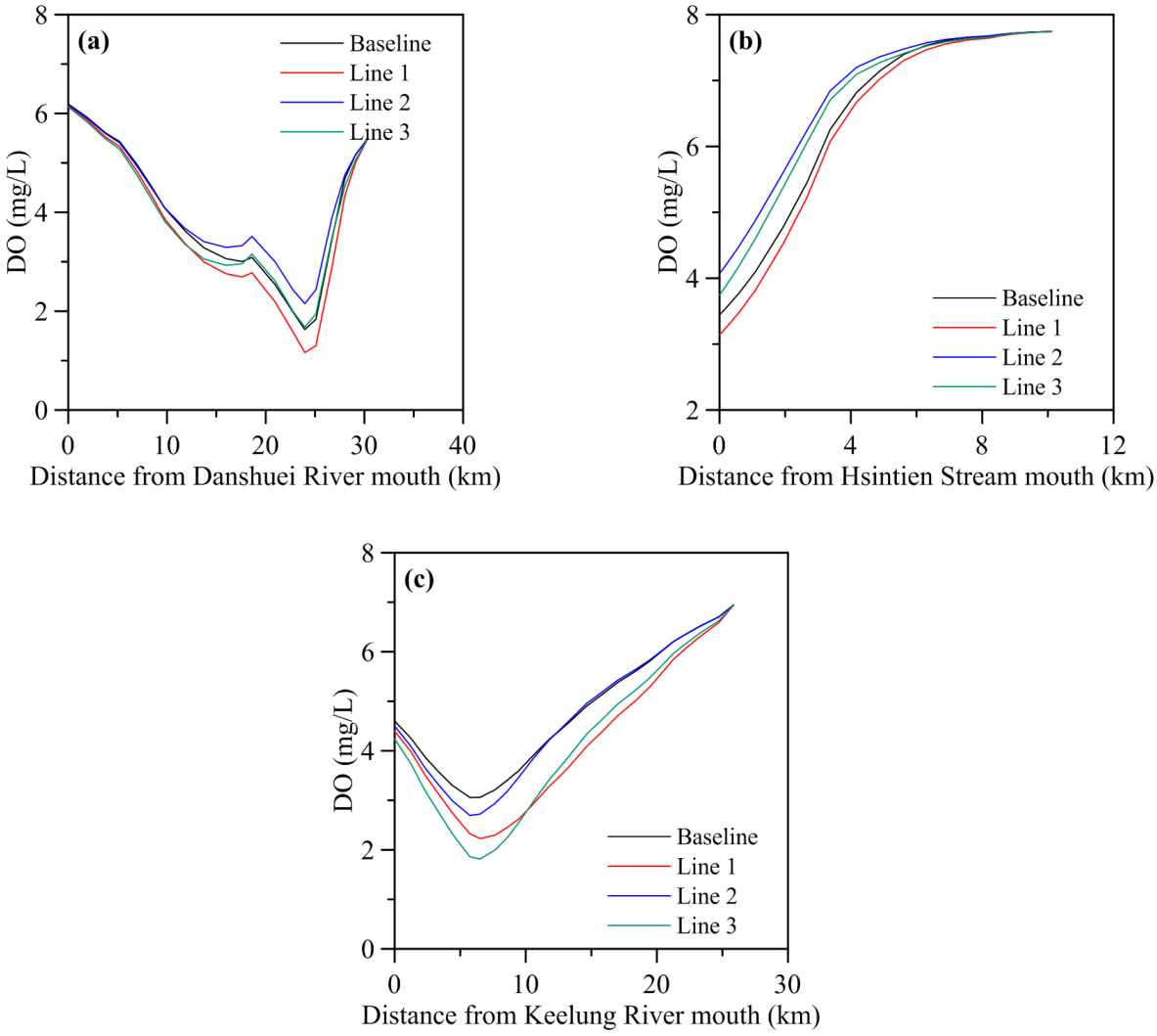

The prediction of dissolved oxygen concentration for Scenario 1 at different locations is provided in Figure 9. A 10% incremental ratio in the nonpoint source was conducted for each model simulation, which demonstrated that the dissolved oxygen decreased as the nonpoint source increased. A linear regression was performed at each location. We determined that a high determination coefficient was exhibited at each location.

Figure 9. Predicting dissolved oxygen concentration for Scenario 1 at different locations: (**a**) Hsin-Hai Bridge; (**b**) Chung-Cheng Bridge; and (**c**) Nan-Hu Bridge. Note that the incremental ratio of the nonpoint source is 10% for each run. The black point and the solid line represent the model prediction and the regression line, respectively.

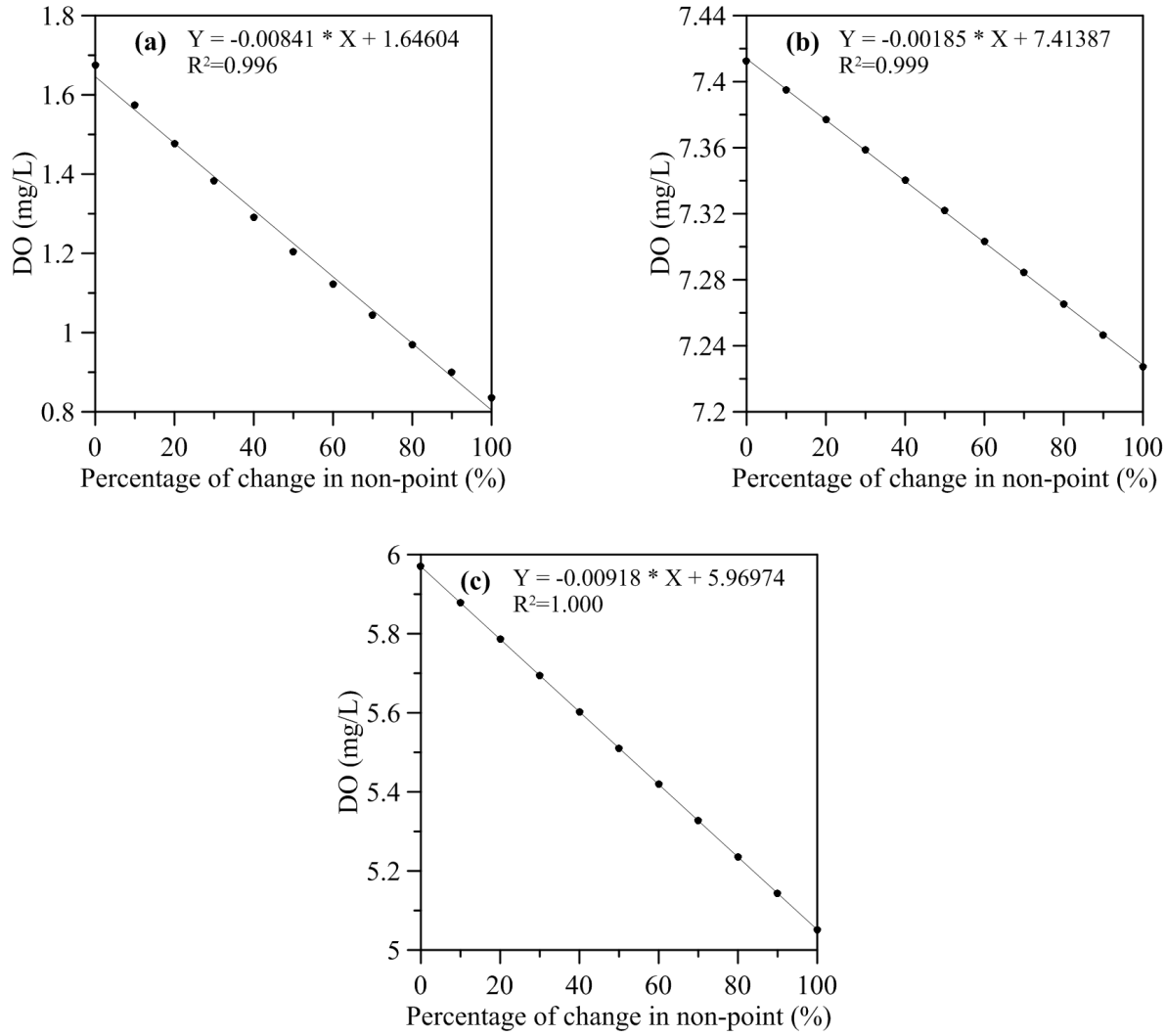

Figure 10 provides the predicted dissolved oxygen concentration for Scenario 2 at three locations. A 10% incremental ratio in the Q_{75} flow was applied to each model simulation. The dashed line in Figure 10 represents the baseline condition. Above and below the dashed line represent the increasing and decreasing dissolved oxygen concentration, respectively. The modeling results indicate that when the Q_{75} flow increases more than 20% under an increasing nonpoint source of 50% at the Hsin-Hai Bridge and the Chung-Cheng Bridge, the dissolved oxygen concentration will be higher than the baseline condition. The Q_{75} flow will increase by at least 50% to overcome a 50% nonpoint source increase and maintain a high dissolved oxygen concentration that is not lower than the baseline condition at the Nan-Hu Bridge.

Figure 10. Predicting dissolved oxygen concentration for Scenario 2 at different locations: (**a**) Hsin-Hai Bridge; (**b**) Chung-Cheng Bridge; and (**c**) Nan-Hu Bridge. Note that the incremental ratio of the Q_{75} flow is 10% for each run. The black point represents the model prediction.

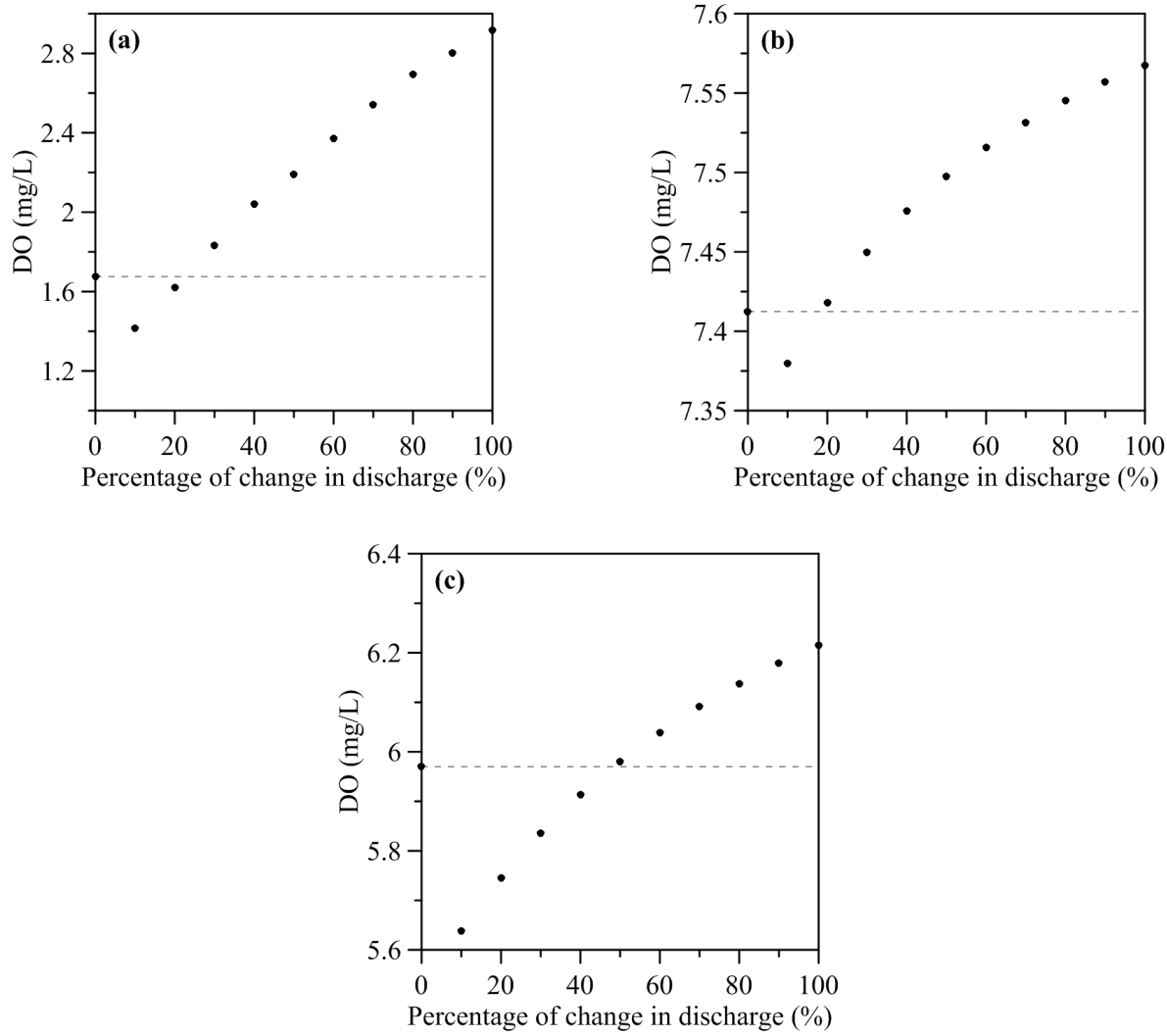

Figure 11 illustrates the predicted dissolved oxygen concentration for Scenario 3 at three locations. The dashed line in Figure 11 also represents the baseline condition. The difference between Scenario 2 and Scenario 3 is the increasing ratio of the nonpoint source. For Scenario 3, the increasing ratio of the nonpoint source is set to 100% (*i.e.*, two-times the nonpoint source). The simulated results indicate that when the Q_{75} flow increases up to 50% and 40% at the Hsin-Hai Bridge and the Chung-Cheng Bridge, respectively, the dissolved oxygen concentration can be higher than the baseline condition. At the Nan-Hu Bridge, the Q_{75} flow increases up to 100% (*i.e.*, two-times the Q_{75} flow) to overcome a 100% increase in the nonpoint source.

Garnier *et al.* [1] used a biogeochemical modeling approach to simulate historical changes in the nutrient delivery and water quality in the Zenne River in Belgium. It was determined that the change in land use could influence the nonpoint source pollution and flow rate and result in a change in water quality, especially the dissolved oxygen concentration in the river. Based on the simulations of

different scenarios in this study, management strategies for water quality can be determined to at least match the dissolved oxygen to the baseline condition.

Figure 11. Predicting dissolved oxygen concentration for Scenario 3 at different locations: (**a**) Hsin-Hai Bridge; (**b**) Chung-Cheng Bridge; and (**c**) Nan-Hu Bridge. Note that the incremental ratio of the Q_{75} flow is 10% for each run. The black point represents the model prediction.

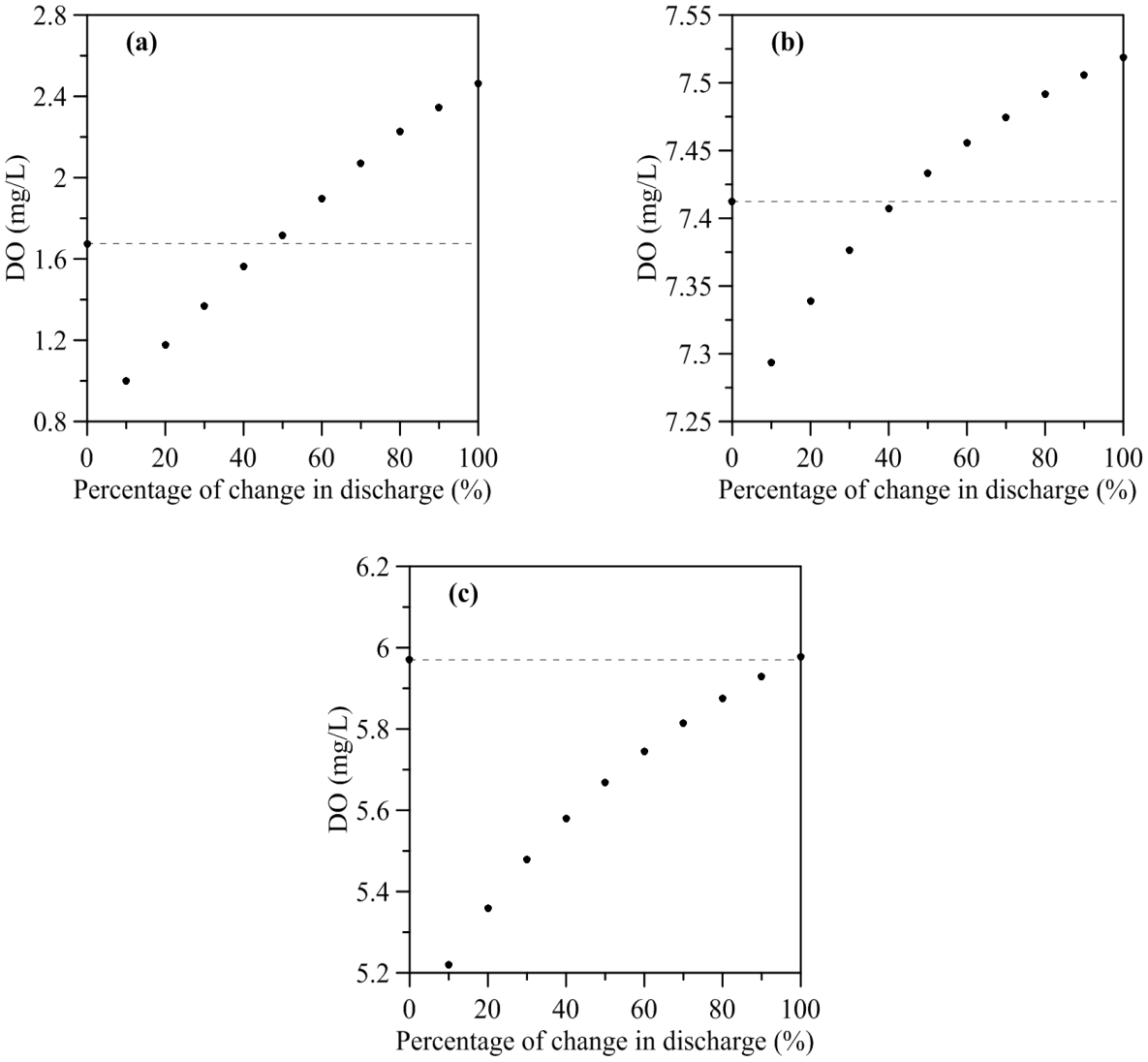

5. Conclusions

A coupled three-dimensional hydrodynamic and water quality model (SELFE-WQ) was applied to the Danshuei River estuary and its adjacent coastal region. The model was validated against the water surface elevation, salinity distribution and water quality variables. The simulated results obtained using the three-dimensional hydrodynamic model indicated that the computed water surface elevation and salinity reproduced the observational data well. The modeling results obtained using the water quality model indicated that the computed water quality parameters, including dissolved oxygen, carbonaceous biochemical oxygen demand, ammonium nitrogen and total phosphorus, mimicked the trends of the

observational data. The overall performance of the model is in qualitative agreement with the available field data.

Then, the validated model was used to assess the system response to a change of nonpoint sources and freshwater discharges from the drainage basin. Three scenarios were investigated to predict the dissolved oxygen distribution in the tidal estuarine system. We determined that an increasing nonpoint source produced a worse water quality, while an increasing freshwater discharge enhanced the dissolved oxygen. The increasing percentage of the nonpoint source and freshwater discharge could produce different simulated results of dissolved oxygen concentration at different locations. However, the effects of combining the nonpoint source and freshwater discharge on dissolved oxygen would result in a nonlinear relationship. The numerical model can provide a useful tool for developing management practices and protecting the water quality in the estuarine system in the future.

In a future study, a watershed model (*i.e*., Soil and Water Assessment Tool, SWAT) can be used to predict flow and nonpoint source loading and then coupled with a hydrodynamic and water quality model to more accurately assess the influence of land use change on water quality in a tidal estuarine system.

Acknowledgments

This study was supported in part by Taiwan's National Science Council under Grant No. 102-2625-M-239-002. This financial support is greatly appreciated. The authors also thank the Taiwan Water Resources Agency, Central Weather Bureau and Environmental Protection Administration for providing the observed data that was used in our model validation.

Author Contributions

Wen-Cheng Liu supervised the progress of the National Science Council (NSC) project and served as a general editor. Wen-Ting Chan performed the model simulations and discussed the results with Wen-Cheng Liu.

Conflicts of Interest

The authors declare no conflict of interest.

References

1. Garnier, J.; Brion, N.; Callens, J.; Passy, P.; Deligne, C.; Billen, G.; Servais, P.; Billen, C. Modeling historical changes in nutrient delivery and water quality of the Zenne River (1790s–2010): The role of land use, waterscape and urban wastewater management. *J. Mar. Syst*. **2013**, *128*, 62–76.
2. Bouraoui, F.; Grizzetti, B. Long term change of nutrient concentration of rivers discharging in European seas. *Sci. Total Environ.* **2011**, *409*, 4899–4916.
3. Sutton, M.; Howard, C.; Erisman, J.W.; Billen, G.; Bleeker, A.; Grennfelt, P.; van Grinsven, H.; Grizzetti, B. *The European Nitrogen Assessment: Sources, Effects and Policy Perspectives*; Cambridge University Press: New York, USA, 2011; p. 601.

4. Buck, O.; Niyogi, D.K.; Townsend, C.R. Scale-dependence of land use effects on water quality of stream in agricultural catchments. *Environ. Pollut*. **2004**, *130*, 287–299.
5. Li, S.; Gu, S.; Liu, W.; Han, H.; Zhang, Q. Water quality in relation to the land use and land cover in the upper Han River basin, China. *Catena* **2008**, *75*, 216–222.
6. Catherine, A.; Mouillot, D.; Maloufi, S.; Troussellier, M.; Bernard, C. Projecting the impact of regional and-use change and water management policies on lake water quality: an application to Periurban Lakes and Reservoirs. *PloS One* **2013**, *8*, 1–11.
7. Silva, L.; Williams, D. Buffer zone versus whole catchment approaches to studying land use impact on river water quality. *Water Res*. **2001**, *35*, 3462–3472.
8. Turner, R.E.; Rabalais, N.N. Linking landscpe and water quality in the Mississippi River Basin for 200 years. *Biosceince* **2003**, *53*, 563–572.
9. Ahearn, D.S.; Sheibley, R.S.; Dahlgren, R.A.; Anderson, J.; Tate, K.W. Land use and land cover influence on water quality in the last free-flowing river draining the western Sierra Nevada, California. *J. Hydrol.* **2005**, *313*, 234–247.
10. Li, S.; Gu, S.; Tan, X.; Zhang, Q. Water quality in the upper Han River basin, China: The impacts of land use/land cover in riparian buffer zone. *J. Hazard. Mater*. **2009**, *165*, 317–324.
11. Lancelot, C.; Gypens, N.; Billen, G.; Garnier, J.; Roubeix, V. Linking marine eutrophication to land use: an integrated river-ocean mathematical tool: The Southern Bight of the North Sea over the past 50 years. *J. Mar. Syst*. **2007**, *64*, 216–228.
12. Tavares, A.O.; Pato, R.L.; Magalhaes, M.C. Spatial and temporal land use change and occupation over the last half century in a Peri-urban area. *Appl.Geogr*. **2012**, *34*, 432–444.
13. Lira, P.K.; Tambosi, L.R.; Ewers, R.M.; Metzger, J.P. Land-use andland-cover change in Atlantic Forest landscape. *For. Ecol. Manage*. **2012**, *278*, 80–89.
14. Huang, J.; Li, Q.; Pontius, R.G.; Klemas, V.; Hong, H. Detecting the dynamic linkage between landscape characteristics and water quality in a subtropical coastal watershed, Southeast China. *Environ. Manage*. **2013**, *51*, 32–44.
15. Rojas, C.; Pino, J.; Basnou, C.; Vivanco, M. Assessing land-use and—Cover changes in relation to geographic factors and urban planning in the metropolitan area of Concepcion (Chile). Implications for biodiversity conservation. *Appl. Geogr*. **2013**, *39*, 93–103.
16. Wang, Y.; Wang, P.; Bau, Y.; Tian, Z.; Li, J.; Shao, X.; Mustavich, L.F.; Li, B.L. Assessment of surface water quality via multivariate statistical techniques: A case study of the Songhua River Harbin region, China. *J. Hydro-Environ. Res*. **2013**, *7*, 30–40.
17. Kibena, J.; Nhapi, I.; Gumindoga, W. Assessing the relationships between water quality parameters and changes in landuse patterns in the Upper Manyame River, Zimbabwe. *Phys, Chem. Earth* **2014**, *67–69*, 153–163.
18. Bu, H.; Meng, W.; Zhang, Y.; Wan, J. Relationships between land use patterns and water quality in the Taizi River Basin, China. *Ecol. Indic*. **2014**, *41*, 187–197.
19. Erol, A.; Randhir, T.O. Watershed ecosystem modeling of land-use impacts on water quality. *Ecol. Model*. **2013**, *270*, 54–63.
20. Wild-Allen, K.; Skerratt, J.; Whitehead, J.; Rizwi, F.; Parslow, J. Mechanisms driving estuarine water quality: A 3D biogeochemical model for informed management. *Estuar. Coast. Shelf Sci.* **2013**, *135*, 33–45.

21. Wan, Y.; Qiu, C.; Doering, P.; Ashton, M.; Sun, D.; Coley, T. Modeling residence time with a three-dimensional hydrodynamic model: Linkage with chlorophyll *a* in a subtropical estuary. *Ecol. Model.* **2013**, *268*, 93–102.
22. Jones, E.M.; Oke, P.R.; Rizwi, F.; Murray, L. Assimilation of glider and mooring data into a coastal and ocean model. *Ocean Model.* **2012**, *47*, 1–13.
23. Weber, T.; Deutsch, C. Oceanic nitrogen reservoir regulated by plankton diversity and ocean circulation. *Nature* **2012**, *489*, 419–422.
24. Lin, Y.P.; Hong, N.M.; Wu, P.J.; Wu, C.F.; Verbug, P.H. Impacts of land use change scenarios on hydrology and land use patterns in the Wu-Tu watershed in Northern Taiwan. *Landsc. Urban Plan*. **2007**, *80*, 111–126.
25. Hsu, M.H.; Kuo, A.Y.; Kuo, J.T.; Liu, W.C. Procedure to calibrate and verify numerical models of estuarine hydrodynamics. *J. Hydrau. Eng. ASCE* **1999**, *125*, 166–182.
26. Liu, W.C.; Hsu, M.H.; Kuo, A.Y. Three-dimensional hydrodynamic and salinity transport modelling of Danshuei River estuarine system and adjacent coastal sea, Taiwan. *Hydrol. Process*. **2007**, *21*, 3057–3071.
27. Zhang, Y.L.; Baptista, A.M. SELFE: A semi-implicit Eulerian-Lagrangian finite-element model for cross-scale ocean circulation. *Ocean Model.* **2008**, *21*, 71–96.
28. Shchepetkin, A.F.; McWilliams, J.C. A method for computing horizontal pressure-gradient force in an oceanic model with a nonaligned vertical coordinate. *J. Geophys. Res*. **2003**, *108*, doi:10.1029/2001JC001047.
29. Umlauf, L.; Buchard, H. A generic length-scale equation for geophysical turbulence models. *J. Mar. Res*. **2003**, *61*, 235–265.
30. Ambrose, R.B., Jr.; Wool, T.A.; Martin, J.L. *The Water Quality Analysis Simulation Program, WASP5, Part A: Model Documentation*; U.S. Environmental Protection Agency: Athens, GA, USA, 1993; p. 202.
31. Chen, C.H.; Lung, W.S.; Li, S.W.; Lin, C.F. Technical challenges with BOD/DO modeling of rivers in Taiwan. *J. Hydro-Environm. Res.* **2012**, *6*, 3–8.
32. Montgomery Watson Harza (MWH). *Evaluation of hydrodynamics and water quality monitoring and management in the Danshuei River basin of New Taipei City*; New Taipei City Government: New Taipei, Taiwan, 2011.
33. Bowie, G.L.; Mills, W.B.; Porcella, D.B.; Campbell, J.R.; Pagenkopf, J.R.; Rupp, G.L. *Rates, Constants, and Kinetics Formulations in Surface Water Quality Modeling*, 2nd ed.; EPA/600/3-85/040; Environmental Research Laboratory, Office of Research and Development, US Environmental Protection Agency: Athens, GA, USA, 1985; p. 455.